AAS 12-243

USING KANE'S METHOD TO INCORPORATE ATTITUDE DYNAMICS IN THE CIRCULAR RESTRICTED THREE BODY PROBLEM

Amanda J. Knutson[*], and Kathleen C. Howell[†]

The model framework developed in this investigation yields the fully coupled equations of motion that govern orbital motion and spacecraft orientation within the context of the circular restricted three body problem. The motion of a spacecraft, composed of two rigid bodies connected by a single degree of freedom joint, is examined. The nonlinear variational form of the equations of motion is employed to mitigate numerical effects caused by large discrepancies in the length scales. Several nonlinear, planar, periodic reference orbits in the vicinity of the collinear libration points are selected as case studies and the effects of the orbit on the orientation, and orientation on the orbit are examined.

INTRODUCTION

The Circular Restricted Three Body Problem (CR3BP) has been examined extensively in recent years; however, considerably fewer studies incorporate the effects of spacecraft attitude in this regime. Numerous missions in the vicinity of the collinear libration points have been completed, are ongoing, or are planned for the near future.[1–3] For example, the James Webb Space Telescope (JWST), successor to the Hubble Telescope, is to be deployed in a Sun-Earth L_2 Lissajous orbit in the next decade.[4] Due to the sensitive nature of the dynamics at the libration points, a better understanding of the attitude motion of spacecraft in the vicinity of these points is desired. The ability to predict the attitude motion of a spacecraft as orbital parameters and spacecraft characteristics are varied can be very useful. Once the behavior is investigated, the possibility of exploiting the natural dynamics for passive attitude control in these regimes is an option. Furthermore, it is desired to examine the coupling effects between orbital motion and orientation in such orbits, to gain a better understanding of the system dynamics. Coupling effects are important when dealing with large spacecraft and could prove useful in the application of solar sails. These issues combine to provide motivation for the development of a novel method to incorporate the effects of attitude dynamics into the CR3BP.

Kane and Marsh first consider the attitude stability of a symmetric satellite, located exactly at the equilibrium points.[5] In their analysis, the satellite is artificially maintained at the equilibrium points and only the attitude motion is considered. Robinson continues this work with an examination of the attitude motion of both a dumbbell satellite[6] and an asymmetric rigid body[7] artificially held at the

[*]Ph.D. Candidate, School of Aeronautics and Astronautics, Purdue University, Armstrong Hall of Engineering, 701 W. Stadium Ave., West Lafayette, Indiana 47907-2045.

[†]Hsu Lo Professor of Aeronautical and Astronautical Engineering, School of Aeronautics and Astronautics, Purdue University, Armstrong Hall of Engineering, 701 W. Stadium Ave., West Lafayette, Indiana 47907-2045. Fellow AAS; Associate Fellow AIAA.

equilibrium points. Abad et al. introduce the use of Euler parameters in the study of a single rigid body located at L_4.[8] More recently, Brucker et al. explore the dynamics and stability of a single rigid body spacecraft in the vicinity of the collinear points in the Sun-Earth system, using Poincaré maps.[9] The effects of the gravity gradient torque are explored by the authors, but the spacecraft is still artificially fixed to the equilibrium point.

Wong et al. examine the motion of a single rigid body near the vicinity of the Sun-Earth libration points in detail, using linear Lyapunov and halo orbit approximations.[10] The work by Wong et al. presents the response of the spacecraft in a meaningful manner, offering orientation results for a number of numerical simulations in terms of a body 3-2-1 (θ, ϕ, ψ) Euler angle rotation sequence. However, since the Lyapunov and halo orbits are represented in a linear form, the simulations are only valid for relatively small orbits close to the equilibrium points. The behavior of multibody spacecraft in the circular restricted three body problem has not been fully explored. Additionally, none of the previous investigations consider the orbit and attitude coupling effects in the CR3BP. Thus, the motivation for the current effort is a more extensive model to explore the orbit-attitude coupling as well as the dynamical influence on the attitude motion in a nonlinear regime.

Selection of a dynamical formulation is an important first step in the development of a model framework to fully couple the orbital mechanics and the attitude dynamics. The equations of motion governing the orbit as well as the spacecraft attitude are brought together in a cohesive manner that minimizes computational difficulties and allows for the propagation of meaningful results. One of the major computational issues in this process is the management of the disparity in length scales in this problem. The distance from the barycenter to the spacecraft is on the order of hundreds of thousands of km (depending on the system), and the spacecraft dimensions are typically measured in terms of meters. The differences in the lengths present a challenge to current computational capabilities, as only finite precision is possible. A nonlinear variational form of the equations of motion is employed to mitigate these numerical effects. The motion of the spacecraft is also monitored relative to some known reference orbit. The time rate of change of linear momentum equations are first used to describe the absolute motion of the spacecraft and then again employed to describe the motion of the reference system. The contributions from the reference are subtracted from the absolute motion, eliminating the difficulties of significantly different lengths coupled within the same differential equations. The specific spacecraft configuration and reference orbits are initially defined and the framework is detailed.

SPACECRAFT MODEL

The spacecraft model is comprised of two generally asymmetric rigid bodies, that is, body B and body R. Two coordinate frames are assigned to the spacecraft. The first coordinate frame is fixed in body B, denoted the b-frame. The second set of unit vectors is fixed in body R and is denoted the r-frame. The coordinate systems align with the principal directions of the individual bodies for each center of mass. The mass of body B is m_b and the center of mass location is denoted B^*. The mass of body R is m_r and the center of mass location is denoted R^*. The inertia matrices corresponding to the two bodies are expressed in terms of b-frame and r-frame coordinates, respectively,

$$I^{B/B^*} = \begin{bmatrix} I_{b_1b_1} & 0 & 0 \\ 0 & I_{b_2b_2} & 0 \\ 0 & 0 & I_{b_3b_3} \end{bmatrix} \qquad I^{R/R^*} = \begin{bmatrix} I_{r_1r_1} & 0 & 0 \\ 0 & I_{r_2r_2} & 0 \\ 0 & 0 & I_{r_3r_3} \end{bmatrix} \tag{1}$$

The two bodies are connected by a revolute joint with a single degree of freedom parallel to the $\hat{b}_3$ direction. Thus, the $\hat{b}_3$ and $\hat{r}_3$ directions are aligned for all time. The location of the joint, denoted J, is specified relative to the centers of mass of each body. In the b-frame, the vector from B^* to J is defined as $\bar{r}^{J/B^*} = s_1\hat{b}_1 + s_2\hat{b}_2 + s_3\hat{b}_3$. In the r-frame, the vector from J to R^* is expressed by $\bar{r}^{R^*/J} = j_1\hat{r}_1 + j_2\hat{r}_2 + j_3\hat{r}_3$. A schematic representation of the spacecraft model is illustrated in Figure 1.

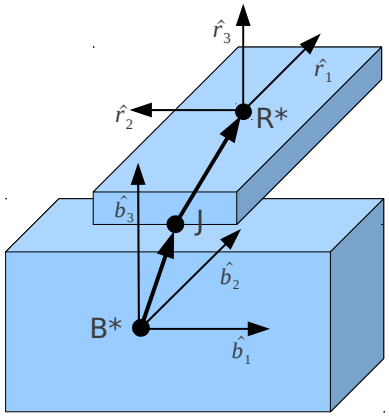

Figure 1. Spacecraft Model

REFERENCE TRAJECTORY

The reference trajectory for this analysis is a path that reflects the motion of a point mass spacecraft propagated in the CR3BP, where the spacecraft is moving under the gravitational influence of two primary bodies modeled as point masses. There are several underlying assumptions that are significant in this model. Since the particle is assumed to be of infinitesimal mass, the primary orbits are modeled as Keplerian. The two primary bodies then move in circular orbits about their common barycenter at a constant rate Ω. A rotating coordinate system is assigned, denoted $(\hat{a}_1, \hat{a}_2, \hat{a}_3)$, as depicted in Figure 2. The angular velocity of the a-frame relative to an inertial frame, n, is denoted ${}^n\bar{\omega}^a$ and is equal to $\Omega\hat{a}_3$.

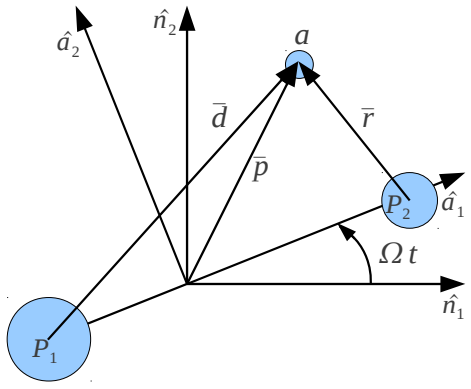

Figure 2. Circular Restricted Three Body Problem

The nondimensional form of the scalar equations of motion for the spacecraft, in the rotating frame $(\hat{a}_1, \hat{a}_2, \hat{a}_3)$, are described below. In nondimensional form, the position vector from the barycenter to the spacecraft center of mass is written $\bar{p} = x\hat{a}_1 + y\hat{a}_2 + z\hat{a}_3$. The symbol μ represents the mass parameter of the specific system considered and is defined as the ratio of the mass of the smaller primary body to the total mass of the two primaries. The resulting scalar nondimensional equations of motion are,

$$\ddot{x} = 2\dot{y} + x - \frac{(1-\mu)(x+\mu)}{d^3} - \frac{\mu(x-1+\mu)}{r^3} \tag{2}$$

$$\ddot{y} = -2\dot{x} + y - \frac{(1-\mu)y}{d^3} - \frac{\mu y}{r^3} \tag{3}$$

$$\ddot{z} = -\frac{(1-\mu)z}{d^3} - \frac{\mu z}{r^3} \tag{4}$$

The CR3BP allows five equilibrium solutions as points relative to the rotating system where the gravitational forces and rotating frame dynamics cancel, assuming a vehicle modeled as a point mass. Two collinear equilibrium points L_1 and L_2 located along the line connecting the two primaries, are of particular interest in this investigation. Both two and three dimensional periodic orbits exist in the vicinity of these points. In-plane, periodic orbits have been computed by differentially correcting initial conditions in the vicinity of each collinear libration point. The EOM in Equations (2) -(4) comprise the model for the motion of the point mass reference body.

DYNAMICAL FORMULATION

The formulation of Kane's equations is explored to model the problem. Kane's method is based on the principles of linear and angular momentum. The method partitions the general formulas for the time rate of change of linear and angular momentum into separate terms in the directions of a set of specified generalized speeds.[11,12] This approach is employed for several reasons. Kane's method is well suited for deriving equations of motion for systems, such as spacecraft, that are composed of many individual bodies connected by joints in a chain or tree-like structure. Kane's method employs simple matrix multiplication methods to derive the equations of motion. Assuming workless constraints, the contact forces are automatically eliminated.[11]

As an alternative to basing the analysis on configuration coordinates (position variables), Kane's method uses velocity variables identified as generalized speeds. The generalized speeds, denoted u_i, are selected in any manner, but it is usually desirable to select an independent set such that changes to one speed do not affect any other speed. If minimal variables are not assigned, constraint equations are incorporated to reduce the order of the system. If minimal variables are selected, one generalized speed is required for each degree of freedom. The total number of generalized speeds is denoted n^*. Some configuration coordinates may be required to fully describe the system. The derivatives of the configuration coordinates are formulated by some combination of a subset of the generalized speeds.

Kane's equations rely on the principles of linear and angular momentum. The following notation is used throughout this investigation. The rate of change of linear momentum, for any body, B, in a system is written,

$$\sum \bar{F}^B - \frac{{}^n d}{dt}\left(m_b {}^n\bar{v}^{B^*}\right) = \bar{0} \tag{5}$$

The sum of all the external forces on body B is then equal to the resultant $\sum \bar{F}^B$. The mass for any body, B, is defined by the scalar quantity m_b. The single overbar denotes a vector. A similar expression yields the rate of change of angular momentum,

$$\sum \bar{M}^{B/B^*} - \frac{^n d}{dt}\left(\bar{\bar{I}}^{B/B^*} \cdot {}^n\bar{\omega}^b\right) = \bar{0} \tag{6}$$

The sum of all external moments on body B about the center of mass, B^*, is represented by the resultant sum $\sum \bar{M}^{B/B^*}$. The double overbar represents a dyadic. Then, $\bar{\bar{I}}^{B/B^*}$ is the inertia dyadic relative to B^* for any three dimensional body. The components of the inertia dyadic are frequently collected in a matrix as,

$$I^{B/B^*} = \begin{bmatrix} I_{b_1b_1} & I_{b_1b_2} & I_{b_1b_3} \\ I_{b_2b_1} & I_{b_2b_2} & I_{b_2b_3} \\ I_{b_3b_1} & I_{b_3b_2} & I_{b_3b_3} \end{bmatrix} \tag{7}$$

where the vector basis is identified prior to computation. The mass moments of inertia of body B, about the center of mass, B^*, are described by $I_{b_1b_1}$, $I_{b_2b_2}$, and $I_{b_3b_3}$, and the remaining terms are products of inertia. Equations (5) and (6) are then used to formulate Kane's equations.

EQUATIONS OF MOTION

Generalized Speeds and Configuration Coordinates

To develop the equations of motion governing the behavior of the spacecraft, generalized speeds are first assigned. The two body spacecraft possesses seven degrees of freedom; therefore seven independent generalized speeds, u_i, are selected. The angular velocity of the b-frame with respect to the a-frame is expressed,

$${}^a\bar{\omega}^b = u_1\hat{b}_1 + u_2\hat{b}_2 + u_3\hat{b}_3 \tag{8}$$

Similarly, an expression for the angular velocity of the r-frame with respect to the b-frame is formulated,

$${}^b\bar{\omega}^r = u_4\hat{b}_3 \tag{9}$$

The remaining generalized speeds are used to describe the translational velocity of B^*, i.e, the center of mass of body B, relative to the current location in the reference orbit, denoted by O

$${}^n\bar{v}^{B^*/O} = u_5\hat{b}_1 + u_6\hat{b}_2 + u_7\hat{b}_3 \tag{10}$$

Several other configuration coordinates are also required to fully describe the system translation and orientation. Euler parameters, as elements in a four-vector, are selected to describe the orientation of the b-frame with respect to the a-frame. The Euler vector is defined,

$${}^a\bar{\epsilon}^b = \epsilon_1\hat{b}_1 + \epsilon_2\hat{b}_2 + \epsilon_3\hat{b}_3 \qquad \text{with the constraint} \qquad {\epsilon_1}^2 + {\epsilon_2}^2 + {\epsilon_3}^2 + {\epsilon_4}^2 = 1 \tag{11}$$

For visualization purposes, it is sometimes desirable to convert the Euler parameter representation of the orientation to an Euler angle rotation sequence. To compare with the results presented by Wong et al., a body 3-2-1 (θ, ϕ, ψ) sequence is implemented to represent the rotation from the a-frame to the b-frame, and is denoted ${C_{ab}}^{\text{3-2-1}}$, i.e.,

$$ {C_{ab}}^{\text{3-2-1}} = \begin{bmatrix} \cos\theta\cos\phi & \cos\theta\sin\phi\sin\psi - \sin\theta\cos\psi & \cos\theta\sin\phi\cos\psi + \sin\theta\sin\psi \\ \sin\theta\cos\phi & \sin\theta\sin\phi\sin\psi + \cos\theta\cos\psi & \sin\theta\sin\phi\cos\psi - \cos\theta\sin\psi \\ -\sin\phi & \cos\phi\sin\psi & \cos\phi\cos\psi \end{bmatrix} \tag{12} $$

For an axisymmetric spacecraft, a body 3-2-3 (α, ζ, γ) sequence, denoted ${C_{ab}}^{\text{3-2-3}}$, is convenient to gain insight about the motion of the b-frame relative to the a-frame. In this form, the angle α indicates precession of the b-frame relative to the a frame, the angle ζ represents nutation, and the angle γ reflects the spin about the axisymmetic axis. This rotation is determined by the direction cosine matrix,

$$ {C_{ab}}^{\text{3-2-3}} = \begin{bmatrix} \cos\alpha\cos\zeta\cos\gamma - \sin\alpha\sin\gamma & -\cos\alpha\cos\zeta\sin\gamma - \sin\alpha\cos\gamma & \cos\alpha\sin\zeta \\ \sin\alpha\cos\zeta\cos\gamma + \cos\alpha\sin\gamma & -\sin\alpha\cos\zeta\sin\gamma + \cos\alpha\cos\gamma & \sin\alpha\sin\zeta \\ -\sin\zeta\cos\gamma & \sin\zeta\sin\gamma & \cos\zeta \end{bmatrix} \tag{13} $$

Kinematic differential equations are employed to determine the Euler parameter rates and are formulated from the following expression.[12]

$$ {}^a\dot{\bar{\epsilon}}^b = \frac{1}{2}\,{}^a\widetilde{\omega}^b E^T \tag{14} $$

where

$$ {}^a\widetilde{\omega}^b = \begin{bmatrix} {}^a\omega_1^b & {}^a\omega_2^b & {}^a\omega_3^b & 0 \end{bmatrix} \qquad \text{and} \qquad E = \begin{bmatrix} \epsilon_4 & -\epsilon_3 & \epsilon_2 & \epsilon_1 \\ \epsilon_3 & \epsilon_4 & -\epsilon_1 & \epsilon_2 \\ -\epsilon_2 & \epsilon_1 & \epsilon_4 & \epsilon_3 \\ -\epsilon_1 & -\epsilon_2 & -\epsilon_3 & \epsilon_4 \end{bmatrix} \tag{15} $$

The angular velocity of the r-frame, fixed in the second body of the spacecraft, relative to the b-frame is integrated directly to yield the angle between these frames. The direction cosine matrix to convert from the b-frame to the r-frame is described as a rotation about $\hat{b}_3$ as follows,

$$ C_{br} = \begin{bmatrix} \cos\beta & -\sin\beta & 0 \\ \sin\beta & \cos\beta & 0 \\ 0 & 0 & 1 \end{bmatrix} \tag{16} $$

The position of R^* with respect to B^* is eventually required and is written in b-frame coordinates and evaluated as,

$$ \bar{r}^{R^*/B^*} = \bar{r}^{J/B^*} + \bar{r}^{R^*/J} C_{br}^T \tag{17} $$

To determine the effects of the attitude motion on the orbit, it is assumed that the spacecraft system center of mass, denoted G^*, is offset from the reference trajectory. The following set of scalar variables, as defined in the rotating orbit frame, is used to track the motion of G^* with respect to the current position in the reference orbit, O, that is,

$$\bar{\delta} = g_1\hat{a_1} + g_2\hat{a_2} + g_3\hat{a_3} \tag{18}$$

The current position in the reference orbit is determined by propagating the point mass system forward in time, or by interpolating a known reference path. The motion of the center of mass of the spacecraft system, G^*, is tracked as the simulation proceeds. This quantity is required to determine the contributions of the gravitational potential from the two primaries.

Kinematics

The next step is the computation of the absolute velocity and absolute angular velocity for body B and body R. These quantities are described using the b-frame vector basis. Additionally, since variational force equations are employed, the velocity for the point mass reference system must also be evaluated. The computations are based on the following,

$$^n\bar{v}^{B^*} = \frac{^nd}{dt}\bar{r}^O + {}^n\bar{v}^{B^*/O} \tag{19}$$

$$^n\bar{v}^{R^*} = \frac{^nd}{dt}\bar{r}^O + {}^n\bar{v}^{B^*/O} + \frac{^bd}{dt}\bar{r}^{R^*/B^*} \tag{20}$$

$$^n\bar{v}^O = \frac{^nd}{dt}\bar{r}^O \tag{21}$$

The absolute angular velocity of body B is represented as the angular velocity of the b-frame and similarly the absolute angular velocity of body R is represented as the angular velocity of the r-frame. Recall, from Figure 2, that the angular velocity of the CR3BP rotating frame with respect to the inertial frame is $^n\bar{\omega}^a$. The kinematic expressions developed are then employed to formulate the dynamic equations of motion.

Momentum Principles

The momentum principles introduced in Equations (5) and (6) are now applied. Equation (5) is first employed to form an equation for the total motion of each of the bodies that comprise the multibody spacecraft, and then to write the equation governing the reference point mass system. To remove the undesirable effects of the discrepancies in the length scales, the point mass equation is subtracted from the total motion of body B, yielding the following variational form,

$$\sum(\bar{F}^B - \bar{F}^O) - \frac{^nd}{dt}\left(m_b{}^n\bar{v}^{B^*/O}\right) = \bar{0} \tag{22}$$

Similar expressions are derived for the second body, R. Equation (6) is applied as written since the point mass system includes no inertia properties about the spacecraft center of mass and, therefore, no external moments are applied. External forces and moments are discussed separately below.

External Forces

This model assumes that the net force derived from the gravitational potential due to the two primaries is the only external force applied to the system. The external field force is assumed to be applied to the center of mass of the system, i.e, G^*. An equivalent system is derived for the two individual bodies, B and R by replacing the force applied at G^*, with a force and moment pair applied at each of the centers of mass of the individual bodies. The difference between the location of the center of mass of the system, $\bar{r}^{G^*}$, and the point on the reference, $\bar{r}^O$ is represented by $\bar{\delta}$. Both $\bar{r}^{G^*}$ and $\bar{r}^O$ are defined with base points fixed in the inertial frame at the barycenter of the Earth-Moon system. The gravitational force exerted on the center of mass of the system G^* is represented by $\bar{F}^{G^*}$ and the gravitational force exerted on the point mass reference system at O, is represented by $\bar{F}^O$. The total mass of the spacecraft system of two bodies is defined as m_t and the difference between the two forces is denoted,

$$\Delta\bar{F} = \bar{F}^{G^*} - \bar{F}^O \tag{23}$$

Since the gravitational force applied at the center of mass of the system, G^*, is nearly identical to the gravitational force exerted on the point mass reference system at O, a variational representation ensures that the appropriate precision is maintained. A general implementation of Encke's method is employed to achieve this task.[13] For the following derivation, two attracting bodies are considered; the Earth and the Moon. The subscript e denotes quantities related to the Earth, and the subscript m indicates lunar terms. The distances from the barycenter to the Earth and from the barycenter to the Moon are represented by $\bar{D}_1$ and $\bar{D}_2$. The distance from the Earth to the location on the reference, O is represented by $\bar{D}_{ref}$, and the distance from the Moon to the location on the reference, O is represented by $\bar{R}_{ref}$. The distances from the Earth and the Moon to the center of mass of the spacecraft system, G^*, are denoted $\bar{D}_g$ and $\bar{R}_g$ respectively. Equation (23) is recast using the point mass gravitational model as follows,

$$\Delta\bar{F} = m_t\left(-\frac{\mu_e}{D_g^3}\bar{D}_g - \frac{\mu_m}{R_g^3}\bar{R}_g\right) - m_t\left(-\frac{\mu_e}{D_{ref}^3}\bar{D}_{ref} - \frac{\mu_m}{R_{ref}^3}\bar{R}_{ref}\right) \tag{24}$$

$$\text{where,}\quad \bar{D}_g = \bar{r}^{G^*} - \bar{D}_1,\quad \bar{R}_g = \bar{r}^{G^*} - \bar{D}_2,\quad \bar{D}_{ref} = \bar{r}^O - \bar{D}_1,\quad \text{and}\quad \bar{R}_{ref} = \bar{r}^O - \bar{D}_2 \tag{25}$$

Rearranging the above expressions and incorporating $\bar{\delta} = \bar{r}^{G^*} - \bar{r}^O$ yields,

$$\Delta\bar{F} = \left(-\frac{\mu_e}{D_{ref}^3}\bar{\delta} - \frac{\mu_e}{D_{ref}^3}\left(\frac{D_{ref}^3}{D_g^3} - 1\right)\bar{D}_g - \frac{\mu_m}{R_{ref}^3}\bar{\delta} - \frac{\mu_m}{R_{ref}^3}\left(\frac{R_{ref}^3}{R_g^3} - 1\right)\bar{R}_g\right) m_t \tag{26}$$

Scalar functions, f_e and f_m, are used to represent the differences $(D_{ref}/D_g)^3 - 1$ and $(R_{ref}/R_g)^3 - 1$, respectively. These differences are written in a more convenient form by introducing scalar quantities q_e and q_m,[13]

$$q_e = \frac{\bar{\delta}\cdot\bar{\delta} - 2\bar{\delta}\cdot\bar{D}_g}{\|\bar{D}_g\|^2} \qquad \text{and} \qquad q_m = \frac{\bar{\delta}\cdot\bar{\delta} - 2\bar{\delta}\cdot\bar{R}_g}{\|\bar{R}_g\|^2} \tag{27}$$

The scalar quantities q_e and q_m are now employed to form new representations of f_e and f_m as follows,

$$f_e = \left(q_e \frac{3 + 3q_e + q_e^2}{1 + (1 + q_e)^{3/2}} \right) \qquad f_m = \left(q_m \frac{3 + 3q_m + q_m^2}{1 + (1 + q_m)^{3/2}} \right) \tag{28}$$

This approach produces results that are accurate as long as the actual spacecraft remains close to the reference. The reference may require rectification for certain simulations if the spacecraft center of mass is observed to shift sufficiently far from the reference. The contributions applied to each body individually is determined by partitioning the total mass, m_t, into the mass of the two bodies, m_b and m_r. All force terms are written in the b-frame vector basis.

External Moments

The gravity gradient moment in this problem is delivered by the two primary bodies. For each primary, this moment is derived from the cross product of the distance from the attracting body to the spacecraft and the second order force expansion.[14] These moments are computed in terms of the b-frame vector basis.

Partial Velocities and Partial Angular Velocities

The partial velocity matrix is formed for each body from the partial derivative of the center of mass velocity with respect to each generalized speed. The partial derivative of the velocity vector is evaluated for each generalized speed and this vector quantity is stored as a row in the partial velocity matrix. The matrices are defined below for body B and body R, respectively. The partial velocity matrix and partial angular velocity matrix for both body B and body R are described in terms of the b-frame vector basis. Each matrix has seven rows, one for each generalized speed, and three columns, one for each spatial dimension of the b-frame.

$$\frac{\partial^n \bar{v}^{B^*}}{\partial \bar{u}} = \begin{bmatrix} 0 & 0 & 0 \\ 0 & 0 & 0 \\ 0 & 0 & 0 \\ 0 & 0 & 0 \\ 1 & 0 & 0 \\ 0 & 1 & 0 \\ 0 & 0 & 1 \end{bmatrix} \tag{29}$$

$$\frac{\partial^n \bar{v}^{R^*}}{\partial \bar{u}} = \begin{bmatrix} 0 & -s_3 - j_3 & s_2 + j_1 \sin\beta + j_2 \cos\beta \\ s_3 + j_3 & 0 & -s_1 - j_1 \cos\beta + j_2 \sin\beta \\ -s_2 - j_1 \sin\beta - j_2 \cos\beta & s_1 + j_1 \cos\beta - j_2 \sin\beta & 0 \\ -j_1 \sin\beta - j_2 \cos\beta & j_1 \cos\beta - j_2 \sin\beta & 0 \\ 1 & 0 & 0 \\ 0 & 1 & 0 \\ 0 & 0 & 1 \end{bmatrix} \tag{30}$$

The partial angular velocity matrix for each body also originates from the partial derivative of the angular velocity vector with respect to each generalized speed. As described previously, these

matrices also have seven rows and three columns, and are described in terms of the b-frame vector basis. The matrices for body B and body R, respectively, are summarized as,

$$\frac{\partial^n \bar{\omega}^B}{\partial \bar{u}} = \begin{bmatrix} 1 & 0 & 0 \\ 0 & 1 & 0 \\ 0 & 0 & 1 \\ 0 & 0 & 0 \\ 0 & 0 & 0 \\ 0 & 0 & 0 \\ 0 & 0 & 0 \end{bmatrix} \qquad \frac{\partial^n \bar{\omega}^R}{\partial \bar{u}} = \begin{bmatrix} 1 & 0 & 0 \\ 0 & 1 & 0 \\ 0 & 0 & 1 \\ 0 & 0 & 1 \\ 0 & 0 & 0 \\ 0 & 0 & 0 \\ 0 & 0 & 0 \end{bmatrix} \tag{31}$$

These quantities are then employed in the formation of Kane's equations.

Constructing Kane's Equations

Using the quantities derived previously, the equations of motion are now constructed using Kane's formulation. The partial velocity vectors and the momentum equations are combined to form Kane's equations of motion. The product of the partial velocity matrix and the time rate of change of linear momentum in Equation (5) and the product of the partial angular velocity matrix and the time rate of change of angular momentum in Equation (6) are determined for each body in the system. A coordinate frame fixed in body B is selected as the common vector basis, and the partial velocity and partial angular velocity matrices and Equations (5) and (6) are represented in terms of this frame. For body B, the equations are summarized below,

$$\frac{\partial^n \bar{v}^{B^*}}{\partial \bar{u}} \sum \bar{F}^B - \frac{\partial^n \bar{v}^{B^*}}{\partial \bar{u}} \left\{ \frac{^n d}{dt} \left(m_b \, {}^n \bar{v}^{B^*} \right) \right\} = \bar{0} \tag{32}$$

$$\frac{\partial^n \bar{\omega}^b}{\partial \bar{u}} \sum \bar{M}^{B/B^*} - \frac{\partial^n \bar{\omega}^b}{\partial \bar{u}} \left\{ \frac{^n d}{dt} \left(\bar{\bar{I}}^{B/B^*} \cdot {}^n \bar{\omega}^b \right) \right\} = \bar{0} \tag{33}$$

These two vector equations for body B are now summed to create one vector equation. Kane splits this equation into two sections, generalized inertia forces and generalized active forces. Generalized inertia forces, denoted $\bar{Q}^*$, combine the contribution of the quantities that depend on the time rate of change of both linear and angular momentum, and the generalized active forces, denoted $\bar{Q}$, collect the contributions from external loads. The generalized inertia force and generalized active force for body B are described as follows,

$$\bar{Q}^*_B = -\frac{\partial^n \bar{v}^{B^*}}{\partial \bar{u}} \left\{ \frac{^n d}{dt} \left(m_b \, {}^n \bar{v}^{B^*} \right) \right\} - \frac{\partial^n \bar{\omega}^b}{\partial \bar{u}} \left\{ \frac{^n d}{dt} \left(\bar{\bar{I}}^{B/B^*} \cdot {}^n \bar{\omega}^b \right) \right\} \tag{34}$$

$$\bar{Q}_B = \frac{\partial^n \bar{v}^{B^*}}{\partial \bar{u}} \sum \bar{F}^B + \frac{\partial^n \bar{\omega}^b}{\partial \bar{u}} \sum \bar{M}^{B/B^*} \tag{35}$$

Similar expression are determined for body R. To apply Kane's method to a multibody system, the contributions from each body must be summed to yield a single equation. A coordinate frame fixed in body B remains as the common vector basis, and all contributions are expressed in terms of this

frame. Kane's formulation for a system composed of m^* bodies is represented by the following expression,

$$\sum_{i=1}^{m^*} \bar{Q}^*_{B_i} + \sum_{i=1}^{m^*} \bar{Q}_{B_i} = \bar{0} \tag{36}$$

The generalized inertia forces and generalized active forces, described in Equations (34) and (35), are computed for each body using the partial velocities in Equations (31), (29), and (30), and the appropriate parts of the momentum equations, from Equations (6) and (22). These two quantities are combined for each body, as described in Equation (36). Finally the contributions from the two separate bodies are added to obtain a single equation of motion corresponding to each generalized speed. The governing equations are produced in the form $A\dot{\bar{u}} = \bar{w}$. This system is combined with derivatives for the required configuration coordinates and integrated to obtain the motion of the individual bodies in the system. The equations of motion for the reference orbit are also integrated at the same time and a conserved quantity is monitored to ensure accuracy of the solution.

APPLICATION TO PERIODIC ORBITS IN EARTH-MOON SYSTEM

Given the model framework that has been established, the effects of attitude dynamics in the CR3BP are explored. Results are propagated in the Earth-Moon system using planar Lyapunov orbits as reference orbits about the three collinear points. The orbital initial conditions are differentially corrected to ensure periodic motion for the necessary time intervals (the Lyapunov orbits are numerically continuous for a minimum of 2.5 revolutions).

Unperturbed Asymmetric Rigid Body

A set of planar Lyapunov orbits about L_1 in the Earth-Moon system, in Figure 3, are selected to explore the effects of location in the orbit and orbit size on the vehicle orientation. The amplitude A_y is indicated for each orbit selected. The smallest orbit is described with an amplitude A_y = 36 km and an approximate period of 11 days. In contrast, the largest orbit possesses an amplitude, A_y = 144000 km with an approximate period of 22 days. The nonlinear nature of the larger Lyapunov orbits is clearly visible. The arrow indicates the direction of motion in the orbit.

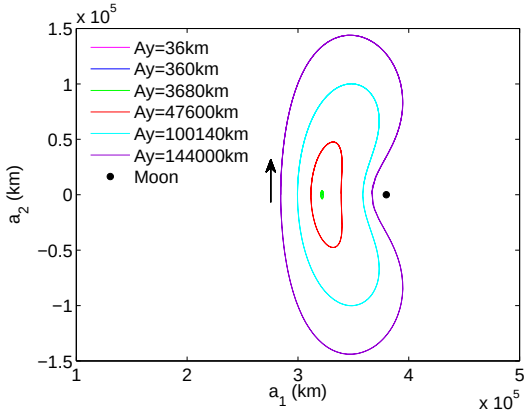

Figure 3. L_1 Planar Lyapunov Reference Orbits in Earth-Moon System

A large rigid asymmetric spacecraft modeled as a single body is tested with the reference orbits described above. The single body spacecraft is achieved by locking the rotational degree of freedom between body B and body R, such that the b-frame and r-frame are aligned for all time. The bodies have equal mass and dimensions of 200 meters in $\hat{b}_1$, 100 meters in $\hat{b}_2$, and 50 meters in $\hat{b}_3$, so that the total system has a mass of 200 kg and dimensions of 200 meters in $\hat{b}_1$, 100 meters in $\hat{b}_2$, and 100 meters in $\hat{b}_3$. The simulation originates with the spacecraft located along the line connecting the two primary bodies, to the left side of L_1 (between the Earth and L_1). No perturbations are applied to the system. The response of the angular velocity of the b-frame with respect to the a-frame in the $\hat{b}_3$ direction is illustrated in Figure 4. A body fixed 3-2-1 (θ, ϕ, ψ) Euler angle sequence is employed to visualize the orientation response. The sequence is employed for asymmetric spacecraft systems for a later comparison with a previous investigation. The response in θ is also displayed. Both ϕ and ψ remain very close to zero throughout the simulation, for all reference orbits considered.

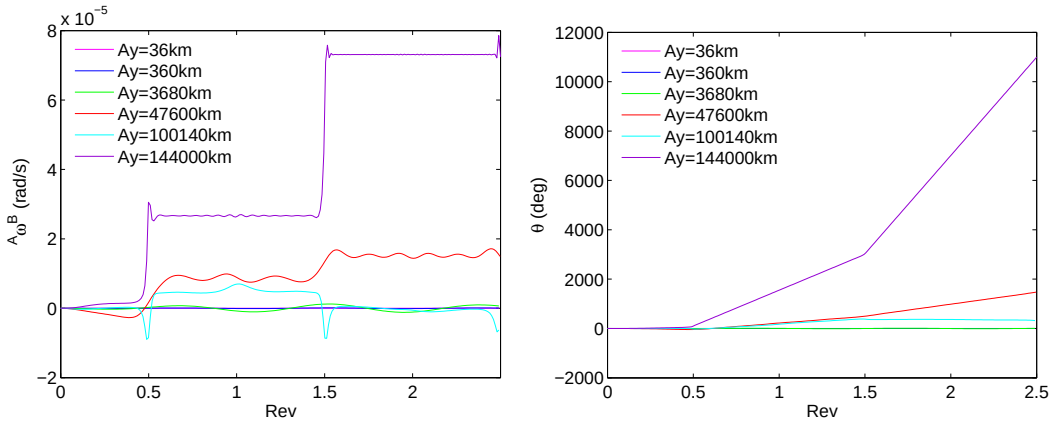

Figure 4. Orientation Response in the Planar L_1 Lyapunov Orbits

The response in the large Lyapunov orbits is clearly dominated by the closest approaches to the second primary, the Moon in this simulation. Both the angular velocity and orientation responses demonstrate sharp changes when the spacecraft is approaching the 0.5 and 1.5 revolutions along the orbit. Further investigation is required to more extensively explore the behavior in the smaller Lyapunov orbits. Two further sets of orbits are displayed in Figure 5. The first set, displayed on the left, aids in examining the behavior in an amplitude range where the linear approximation to the orbit is still reasonable, which appears in the figure to include an A_y less than approximately 4000 km for L_1 Lyapunov orbits in the Earth-Moon system. The A_y values are displayed for each orbit. Examining this plot, it is clear that the orbits are generally elliptical in nature and not dominated by any nonlinear effects. The second set, on the right in Figure 5, offers insight into the capabilities of the linear approximation. The smaller orbits remain elliptical in nature, but as A_y is increased the nonlinear effects emerge.

No perturbations are applied to the system for spacecraft in the new sets of reference trajectories. The response in θ is again displayed in Figure 6, for A_y values less than 50000 km. Both ϕ and ψ remain very close to zero for all reference orbits considered. The left plot demonstrates that the response for the smaller set of orbits is cyclic in nature, with increasing amplitude in θ as the orbit size increases. In these orbits, the spacecraft exhibits a slow oscillatory motion in the out-of-plane direction, which appears to be bounded over the simulation time.

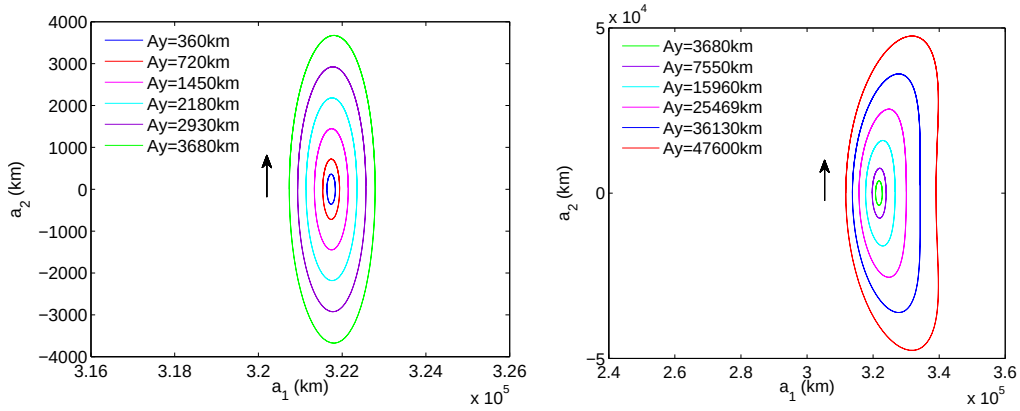

Figure 5. Two Sets of Planar L_1 Lyapunov Orbits

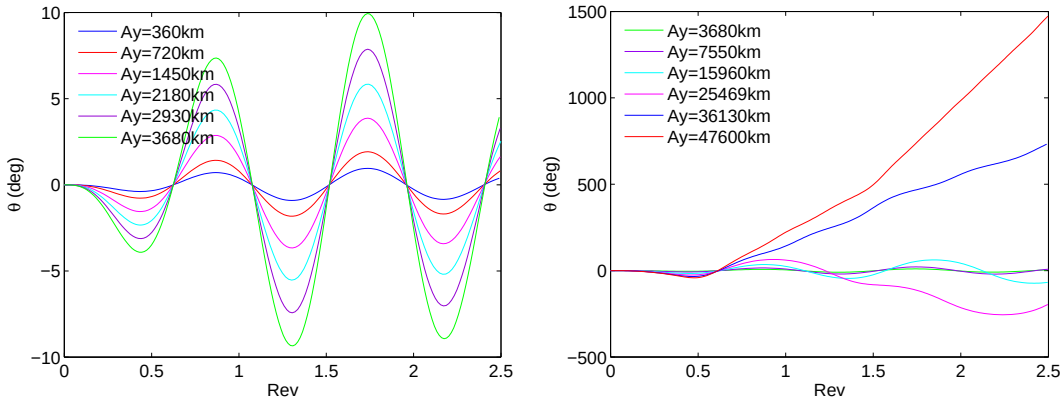

Figure 6. Response in θ for Refined L_1 Planar Lyapunov Orbit Sets

The rotational motion that is observed in the simulation can be better understood by considering the net moment, due to the gravity gradient torque, on the spacecraft at four locations along the planar Lyapunov orbit. Temporarily consider that the spacecraft frame (the b-frame) and the orbit frame (the a-frame) are considered to be aligned at all locations on the orbit. The simulation originates with the spacecraft located along the line connecting the two primary bodies, to the left side of L_1 (between the Earth and L_1). At this location the net moment is zero. The direction of motion in the orbit is clockwise, and after 0.25 revolutions along the Lyapunov, the spacecraft is located at the maximum $\hat{a}_2$ amplitude along the orbit, at (L_1,A_y). The net gravity gradient moment at this location is negative. After 0.5 revolutions of the Lyapunov, the spacecraft is once again located along the line connecting the two primary bodies and is now to the right side of L_1. The net moment at this location is once again zero. The last location considered is at 0.75 revolutions of the Lyapunov orbit, where the spacecraft is located again at the maximum $\hat{a}_2$ amplitude of the orbit at (L_1,$-A_y$). At this location, the net moment is positive. Thus, the angle θ become negative for approximately the first half revolution of the Lyapunov and then reorients to become positive for the second half of the revolution. For each orbit, the period of the oscillation varies slightly over the simulation interval. This frequency response is unaffected by increases in the orbit size. For all the relatively small orbits in this first set, the period of oscillations appear to be slower than the period of the

Lypunov for the first cycle and slightly faster than the Lyapunov period over the second cycle. The plot on the right reflects the response in θ for the orbits with the larger amplitudes. It is clear that the motion becomes unbounded if the Lyapunov size is increased. This appears to coincide with the point at which the linear orbit approximation may break down ($A_y \approx 4000$ km for L_1 Lyapunov orbits in the Earth-Moon system).

Spin Stabilization of Axisymmetric Spacecraft

The model is now used to predict the behavior of an axisymmetric body under an angular velocity perturbation in the $\hat{b}_1$ direction. The spacecraft is composed of two rigid rods, each of length 10 meters and radius 0.1 meter. The rods are stacked on top of each other, configured so that the axial direction is aligned with $\hat{b}_3$. The top rod can spin about $\hat{b}_3$ relative to the bottom rod. This spacecraft is placed in an L_1 planar Lyapunov orbit in the Earth-Moon system with an A_y value of approximately 3680 km. The orientation response is displayed in Figure 7, in terms of the body fixed 3-2-3 (α, ζ, γ) Euler angle sequence, for four test cases. Recall that the angle α represents precession of the b-frame relative to the a frame, the angle ζ represents nutation, and the angle γ represents the spin about the axisymmetic axis.

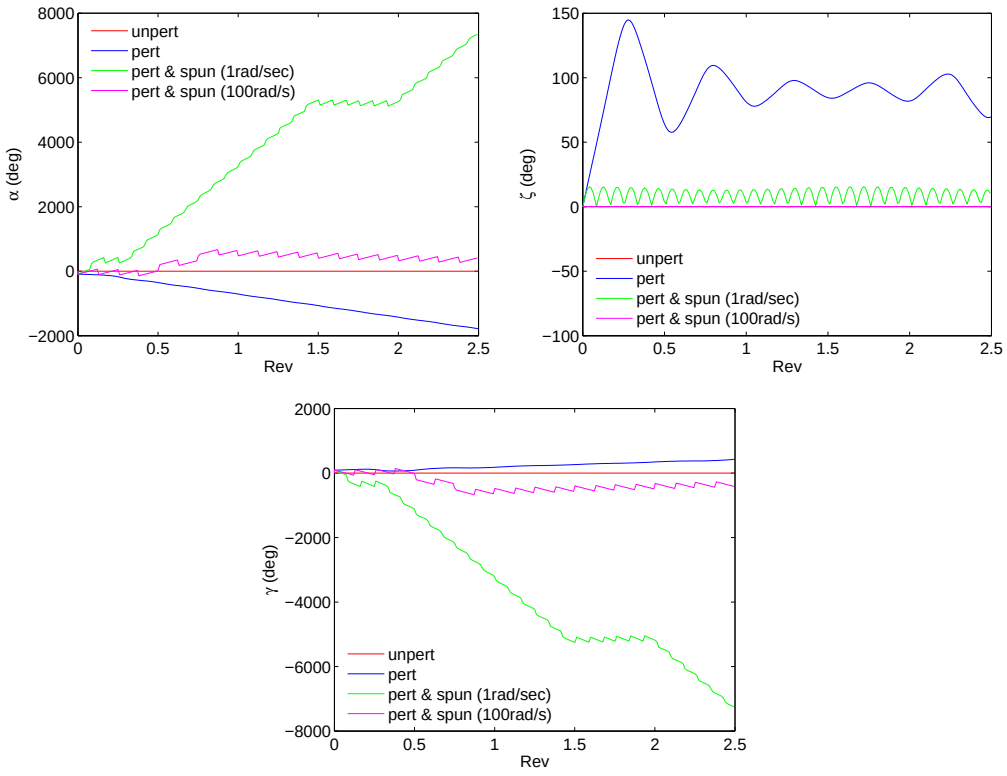

Figure 7. Orientation Response to Spin Stabilization

The unperturbed motion with the rods joined with no relative spin is displayed in red. A perturbation of 0.00001 rad/sec is applied to body B in the $\hat{b}_1$ direction while the rods are still fixed. This perturbation is noted to be 3.75 times the orbital rate of the primaries. This perturbed motion is plotted in blue. Once the perturbation is applied, the rod is observed to fall into the plane of primary motion, as depicted by the nutation angle, α, in Figure 7. This behavior is expected, as the rod is in

an unstable configuration at the beginning of the simulation. Spin stabilization is attempted by spinning body R at a rate of 1 rad/sec in the $\hat{b}_3$ direction and this motion is indicated in green. The effect of increasing the spin rate to 100 rad/sec is also examined, and this response is plotted in magenta. It is apparent in Figure 7 that spin stabilization for this particular perturbation is possible. In response to the perturbed motion, the spacecraft exhibits oscillatory motion in α and unbounded motion in the other two angles which confirms that the spacecraft is not maintaining the initial orientation. Using a spin rate of 1 rad/sec, the nutation angle is observed to be much improved; however, the spacecraft is precessing with respect to the orbit frame at a higher rate then in the perturbed case. By increasing the spin rate to 100 rad/sec, nearly all the effects of the initial perturbation on the nutation angle are damped out, and the precession and spin angles also demonstrate improvement relative to the perturbed case over the length of the simulation. This test case serves two purposes. First, the results confirm that the spacecraft is displaying motion consistent with results observed in the two body problem, which builds confidence in the model formulation. Secondly, it demonstrates that spin stabilization is possible, at least for some orientation parameters, in the CR3BP.

Perturbed Axisymmetric Spacecraft Impact on Orbit

With the fully coupled dynamical model, the effects of an attitude perturbation on the orbit is also examined. The axisymmetric spacecraft is composed of two rigid rods with a length-to-radius ratio of 100:1. The rods are stacked one on top the other, and configured such that the axial direction is aligned with the out-of-plane direction, $\hat{b}_3$. The effects of increasing the length, while maintaining a constant ratio of length-to-radius, are examined for a L_1 planar Lyapunov orbit in the Earth-Moon system with an A_y amplitude of 144000 km. Two sets of perturbations are considered to investigate the coupling effects and the length of the rod is increased from 10 meters to 100000 meters. First, the generalized speed u_1, the angular velocity of the body B in the $\hat{b}_1$ direction, is perturbed from 0 rad/sec to 0.0001 rad/sec (37.5 times the orbital rate). For this perturbation, the deviation of the system center of mass, G^*, relative to the reference trajectory is very small. Secondly, a body fixed 3-2-3 Euler angle rotation sequence (α, ζ, γ) is used to produce an orientation offset of ζ = 5 deg. With no perturbation in ζ, G^* does not move relative to O. For this particular test case, large motions of the center of mass of the spacecraft (G^*) with respect to the location in the reference orbit (O) are observed. The motion of G^* relative to O is displayed in Figure 8 over the first revolution in the Lyapunov orbit, where a change in the response is observed as the spacecraft passes close to the Moon at 0.5 revolutions along the Lyapunov. This effect is repeated in the second revolution of the Lyapunov (presented in Figure 9 when the spacecraft makes another closest approach to the Moon at 1.5 revolutions. Prior to the encounter with the Moon, the spacecraft is observed to be departing the reference orbit. As the spacecraft size increases, the motion of G^* away from the reference location O is noted to also increase. Since the region is very sensitive, fairly small motions in the initial conditions can result in a vehicle that departs the L_1 region significantly earlier than a spacecraft moving along the reference.

The effect of changing the magnitude of the initial perturbation in the orientation angle, ζ, is also explored. The initial perturbation in ζ is increased to 10 deg to investigate how increasing the perturbation size affects the motion of G^* relative to the location in the reference orbit O. Figure 10 displays the response of an axispacecraft of length 10000 m and radius 100m, in a L_1 planar Lyapunov orbit in the Earth-Moon system with an A_y amplitude of 144000 km, for ζ = 0 deg, ζ = 5 deg and ζ = 10 deg. For the three angles examined, the largest response in G^* is observed for the largest perturbation in ζ. Figure 10 also indicates that when there is no perturbation in ζ, the motion of G^* tracks closely to the position in the reference orbit, O.

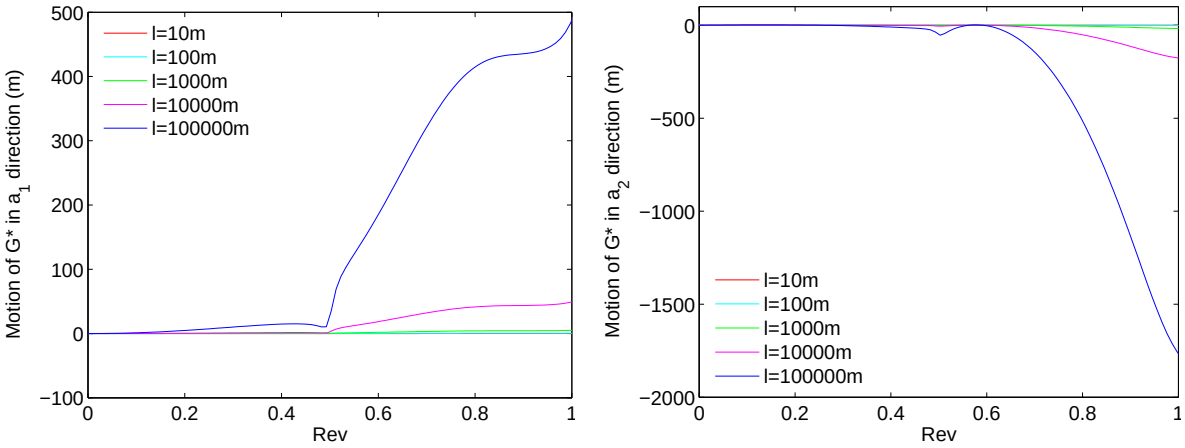

Figure 8. Motion of G^* Relative to O, for ζ = 5 deg, over One Rev of Large E-M Lyapunov

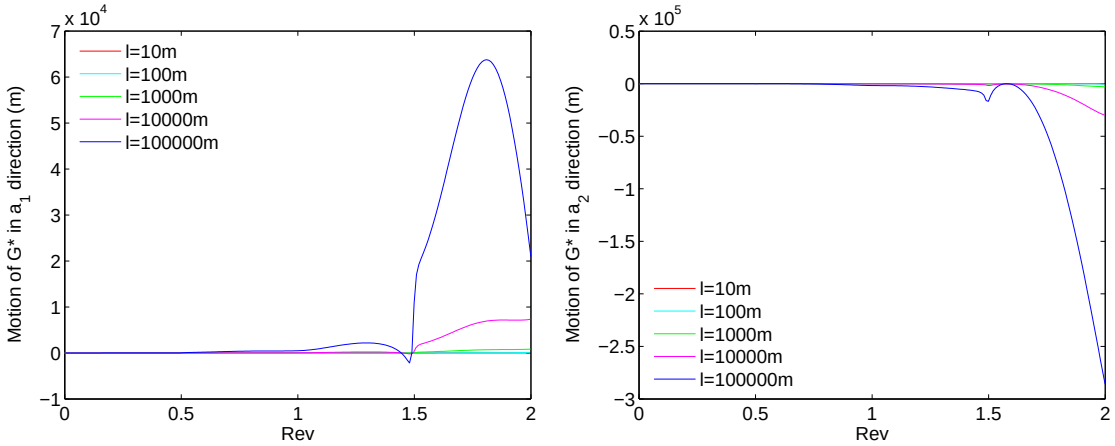

Figure 9. Motion of G^* Relative to O, for ζ = 5 deg, over Two Revs of Large E-M Lyapunov

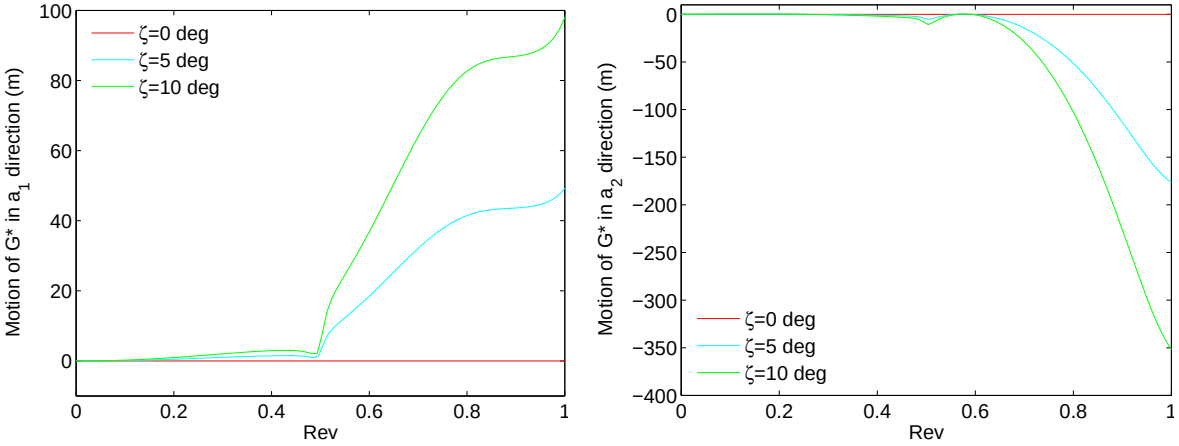

Figure 10. Motion of G^* Relative to O, for ζ = 0 deg, 5 deg, and 10 deg

The effect of decreasing the size of the L_1 planar Lyapunov reference orbit in the Earth-Moon system to an A_y amplitude of 25469 km is considered. An initial perturbation in ζ of 5 deg is applied and the length of the rod is increased from 10 meters to 100000 meters. The motion of G^* relative to O is displayed on the left in Figure 11 over two revolutions in the Lyapunov orbit, where the spacecraft are observed to be departing the vicinity of the Lyapunov reference orbit. Further examination confirms that the spacecraft are departing on the unstable manifold associated with the particular reference considered, as depicted on the right in Figure 11.

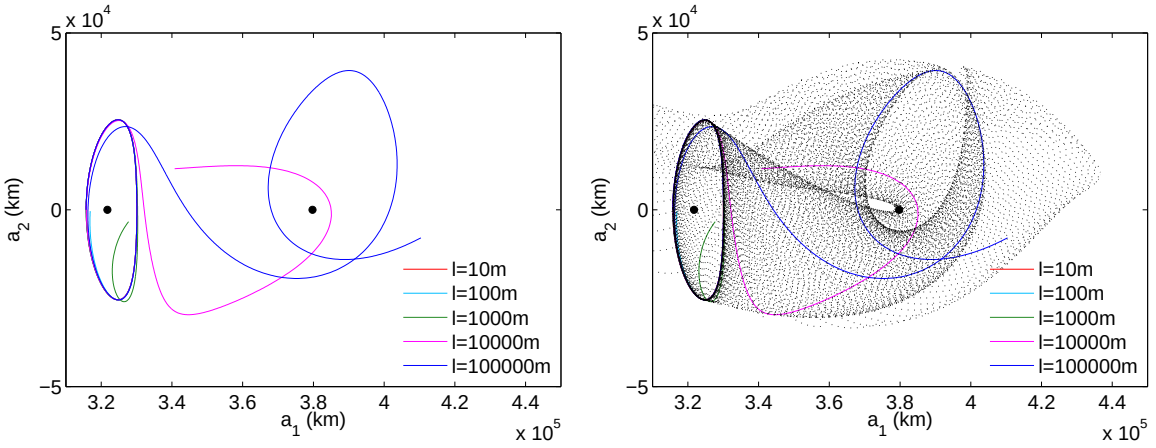

Figure 11. Motion of G^* Relative to O, for ζ = 5 deg, E-M L_1 Lyapunov (A_y = 25469 km)

Perturbed Asymmetric Rigid Body

Wong et al. examine the motion of a single asymmetric rigid body near the vicinity of the Sun-Earth libration points, using linear Lyapunov approximations.[10] The investigation considers motion of the spacecraft center of mass relative to the L_2 libration point and offers orientation results in terms of a body 3-2-1 (θ, ϕ, ψ) Euler angle rotation sequence. The linear orbits are represented analytically, thus, the orbit is not affected by the orientation.

The model framework to couple translational and rotational motion is employed to expand the investigation presented by Wong et al. The motion of an asymmetric rigid body moving in the vicinity of L_2 in the Earth-Moon system is examined. Three different nonlinear planar Lyapunov reference orbits are considered, with approximate A_y values of 125 km, 6500 km, and 13400 km. These orbits are selected for comparison to the results from Wong et al. in the Sun-Earth system.[10] The left plot in Figure 12 represents the nonlinear orbits that correspond to the linear orbits employed in the work by Wong in the Sun-Earth system. The similar nonlinear orbits in the Earth-Moon system are plotted on the right. The orbits in the Earth-Moon system are scaled by the ratio of the distance between the smaller primary and L_2 in the two systems. The arrows indicate the direction of motion in the orbits.

The spacecraft is modeled as a single asymmetric rigid body, with a total mass of 100 kg. The moment of inertia properties in b-frame coordinates for the system are $I_{b_1 b_1}$=7.083 kg·m^2, $I_{b_2 b_2}$=11.333 kg·m^2, and $I_{b_3 b_3}$=12.417 kg·m^2, which are consistent with the quantities employed by Wong et al. All products of inertia are equal to zero. A body fixed 3-2-1 (θ, ϕ, ψ) Euler angle sequence is employed to visualize the orientation response. Propagating the system with no perturbations yields zero response in ϕ or ψ; however, there is a response in the θ, which is amplified as A_y increases.

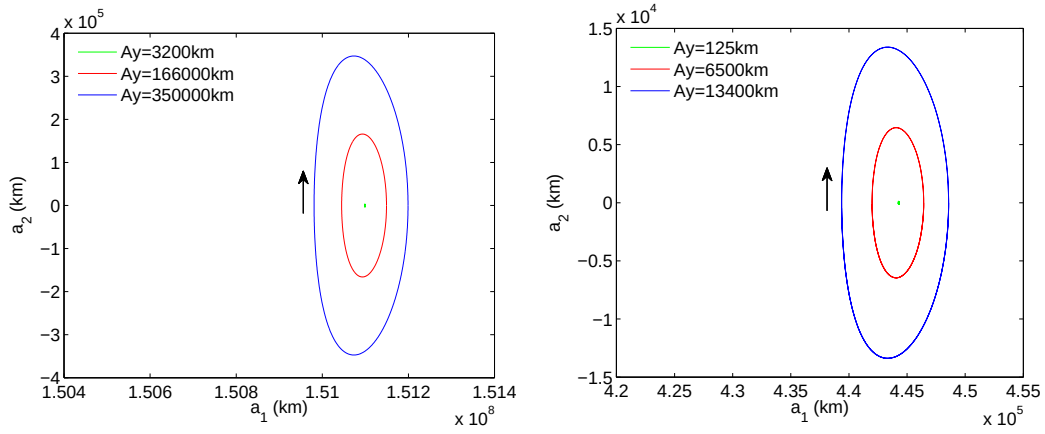

Figure 12. L_2 **Planar Lyapunov Orbit in the Sun-Earth (left) and Earth-Moon (right) Systems**

Two sets of perturbations in (θ, ϕ, ψ) are explored: $(5, 5, 5)$ deg and $(-5, -5, -5)$ deg. The first perturbation set, $(5, 5, 5)$ deg, corresponds to the results presented by Wong et al.[10] The impact on the Euler angles as a result of simulations initialized with the two perturbations sets are displayed in Figure 13. The positive perturbation yields a very similar response to the results that appear in Wong et al., especially for the smaller orbits. As A_y increases, differences are observed between this investigation and the work by Wong et al, likely due to differences in the system and increases in the nonlinear effects of the orbit.

By analyzing the linear attitude equations at the libration points, Wong et al. also identified a critical ratio of inertia values that excite large amplitude motion in θ. For spacecraft in a planar Lyapunov orbit about L_2, modeled as linear, as the value of $k_3 = (I_{b_2b_2} I_{b_1b_1})/I_{b_3b_3}$ approaches a critical value of 0.36 in the Earth-Moon system, the amplitude of θ grows to infinity. Values of k_3 further from the critical value yield a more stable response, assuming that the inertias satisfy the additional condition that $I_{b_3b_3} > I_{b_2b_2} > I_{b_1b_1}$ as noted in the linear analysis by Wong et al.[10] For relatively small orbits, this observation holds over the propagation interval when a nonlinear planar Lyapunov reference is incorporated. The inertia properties in terms of $I_{b_1b_1}$ are modified to supply various k_3 values and the results for an Earth-Moon L_2 orbit (A_y = 125 km) are displayed on the left in Figure 14. The largest response in θ occurs for the k_3 value that is closest to the critical value of 0.36. The amplitude response in θ diminishes for k_3 values below and also above the critical value as expected. However, when larger nonlinear orbits are selected as the reference orbits, large amplitude motion is apparent for a variety of k_3 values. Given the same set of k_3 values, the response in θ for a planar Lyapunov L_2 orbit (A_y = 13400 km) in the Earth-Moon system is plotted on the right in Figure 14. It is clear that the amplitude response in θ is no longer dominated by the critical value of k_3 and the nonlinear effects are significant in the attitude behavior over the propagation interval. It should be noted that there is no motion of the spacecraft system center of mass (G^*) relative to the location in the reference orbit (O) for any k_3 value investigated. Also, unlike the unperturbed rigid asymmetric spacecraft in the large L_1 Earth Moon Lyapunov orbits, the reference orbits are all sufficiently far away from the moon that the behavior is not dominated by a close lunar approach.

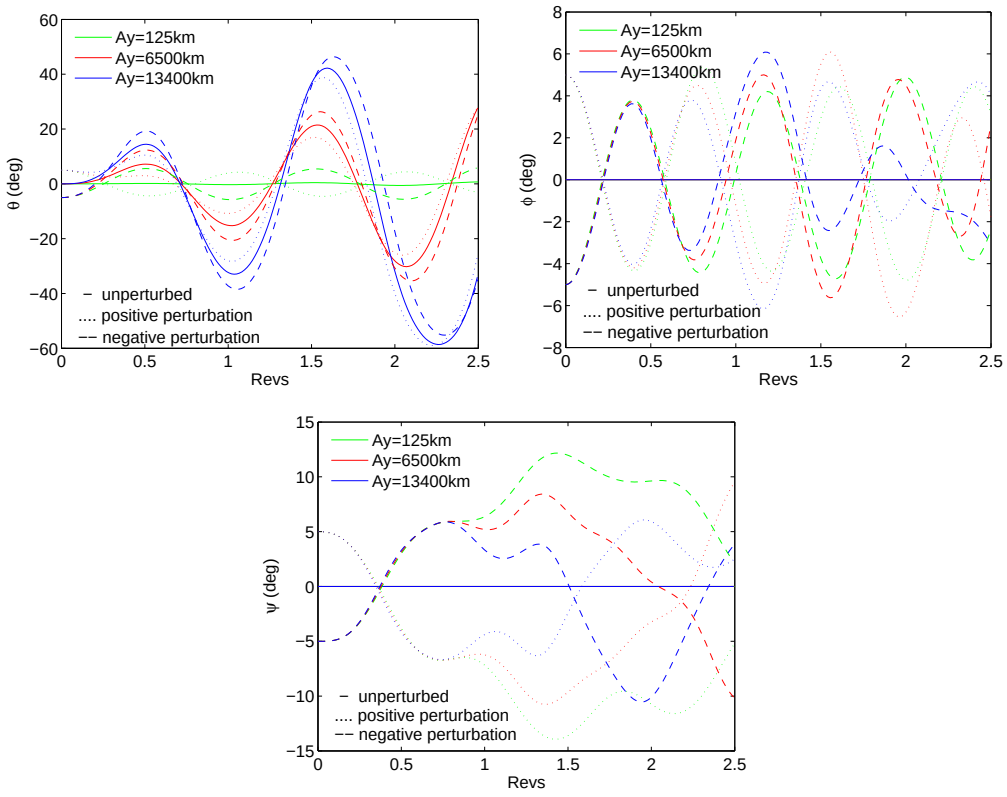

Figure 13. Orientation Response of Asymmetric Rigid Body

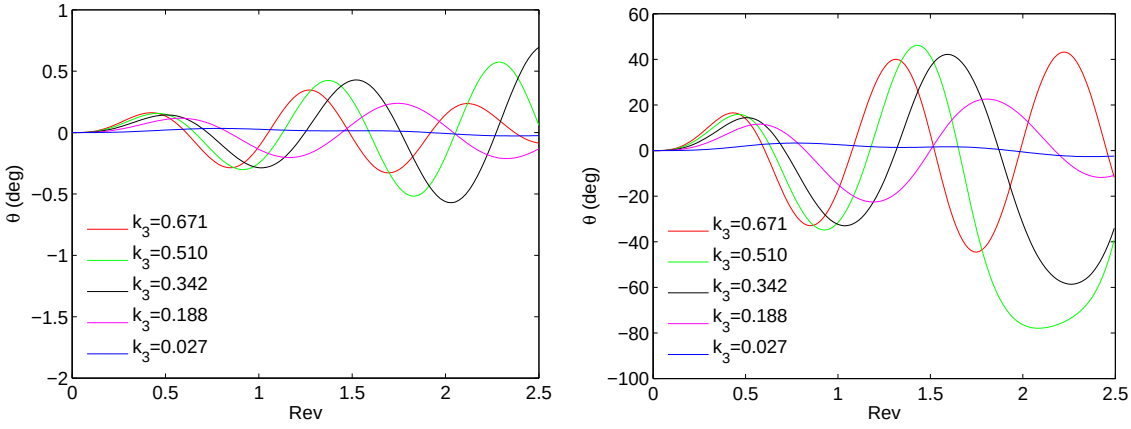

Figure 14. Orientation Response for A_y = 125 km (left) and A_y = 13400 km (right)

SUMMARY

The goals in this investigation include the development a framework to explore attitude dynamics within the context of the circular restricted three body problem, the testing of the framework, and the exploration the nature of the dynamics in this regime with some preliminary examples. The motion of a spacecraft, composed of two rigid bodies connected by a single degree of freedom joint, is examined. The equations of motion governing the orbit as well as the spacecraft attitude are integrated to minimize computational difficulties and to allow for the propagation of meaningful results. The nonlinear variational form of the equations of motion is employed to manage the disparity in length scales. Within this framework, a process is summarized with steps for implementation resulting in a series of coupled nonlinear equations of motion for the complex spacecraft model. The observations from the preliminary case studies display the coupling effects between orbital motion and orientation in this sensitive regime. The attitude behavior displayed in the large, nonlinear reference orbits can be unexpected.

ACKNOWLEDGMENT

We appreciate the support of the Natural Sciences and Engineering Research Council of Canada, Zonta International, and the College of Engineering at Purdue University (School of Aeronautics and Astronautics and School of Engineering Education).

REFERENCES

[1] D. Richardson, "Halo Orbit Formation for the ISEE-3 Mission," *Journal of Guidance and Control*, Vol. 3, No. 6, 1980, pp. 543–448.

[2] 21st International Symposium on Space Flight Dynamics, *ARTEMIS: The First Mission to the Lunar Libration Orbits*, September 28 - October 2 2009.

[3] M. Hechlera, M. Morab, M. Nogalesb, and A. Yezc, "Orbit Concepts at L2 for Soyuz Launches from Kourou," *Acta Astronautica*, Vol. 62, No. 2-3, 2008, pp. 140–150.

[4] D. Folta, "Formation Flying Design and Applications in Weak Stability Boundary Regions," *Annals of the New York Academy of Science*, Vol. 1017, 2004, pp. 95–111.

[5] T. Kane and E. Marsh, "Attitude Stability of a Symmetric Satellite at the Equilibrium Points in the Restricted Three-Body Problem," *Celestial Mechanics*, Vol. 4, 1971, pp. 78–90.

[6] W. Robinson, "The Restricted Problem of Three Bodies with Rigid Dumb-bell Satellite," *Celestial Mechanics*, Vol. 7, 1973, pp. 323–330.

[7] W. Robinson, "Attitude Stability of a Rigid Body Placed at an Equilibrium Point in the Restricted Problem of Three Bodies," *Celestial Mechanics*, Vol. 10, 1974, pp. 17–33.

[8] A. Abad, M. Arribas, and A. Elipe, "On the Attitude of a Spacecraft Near a Lagrange Point," *Publishing House of the Czechoslovak Academy of Science*, Vol. 40, No. 5, 1989, pp. 302–307.

[9] E. Brucker and P. Gurfil, "Analysis of Gravity-Gradient-Perturbed Rotational Dynamics at the Collinear Lagrange Points," *The Journal of Astronautical Sciences*, Vol. 55, No. 3, 2007, pp. 271–291.

[10] B. Wong, R. Patel, and A. Misra, "Attitude Dynamics of Rigid Bodies in the Vicinity of the Lagrangian Points," *Journal of Guidance, Control, and Dynamics*, Vol. 31, No. 1, 2008, pp. 252–256.

[11] T. Kane and D. Levinson, *Dynamics: Theory and Applications*. New York: McGraw Hill, Inc., 1985.

[12] T. Kane, P. Likins, and D. Levinson, *Spacecraft Dynamics*. New York: McGraw Hill, Inc., 1983.

[13] H. Schaub and J. Junkins, *Analytical Mechanics of Space Systems*. Virginia: AIAA, 2003.

[14] P. Hughes, *Spacecraft Attitude Dynamics*. New York: Dover Publications, Inc., 2004.